Magmato-Tectonic Cyclicity at the Ultra-Slow Spreading Southwest Indian Ridge: Evidence from Variations of Axial Volcanic Ridge Morphology and Abyssal Hills Pattern

Véronique Mendel, Daniel Sauter, Céline Rommevaux-Jestin, Philippe Patriat, Fabrice Lefebvre, Lindsay M. Parson

Geochemistry Geophysics Geosystems G3
AN ELECTRONIC JOURNAL OF THE EARTH SCIENCES
Published by AGU and the Geochemical Society

Article
Volume 4, Number 5
10 May 2003
9102, doi:10.1029/2002GC000417
ISSN: 1525-2027

Magmato-tectonic cyclicity at the ultra-slow spreading Southwest Indian Ridge: Evidence from variations of axial volcanic ridge morphology and abyssal hills pattern

V. Mendel and D. Sauter
Institut de Physique du Globe de Strasbourg (CNRS/ULP), 5 rue René Descartes, 67084 Strasbourg, France (veronique.mendel@eost.u-strasbg.fr; daniel.sauter@eost.u-strasbg.fr)

C. Rommevaux-Jestin, P. Patriat, and F. Lefebvre
Institut de Physique du Globe de Paris, 4 place Jussieu, 75252 Paris Cedex 05, France (rommevau@ipgp.jussieu.fr; ppa@ccr.jussieu.fr)

L. M. Parson
Southampton Oceanography Centre, Empress Dock, Southampton SO14 3ZH, United Kingdom (lmp@soc.soton.ac.uk)

[1] On-axis deep tow side scan sonar data are used together with off-axis bathymetric data to investigate the temporal variations of the accretion processes at the ultra-slow spreading Southwest Indian Ridge. Differences in the length and height of the axial volcanic ridges and various degrees of deformation of these volcanic constructions are observed in side scan sonar images of the ridge segments. We interpret these differences as stages in an evolutionary life cycle of axial volcanic ridge development, including periods of volcanic construction and periods of tectonic dismemberment. Using off-axis bathymetric data, we identify numerous abyssal hills with a homogeneous size for each segment. These abyssal hills all display an asymmetric shape, with a steep faulted scarp facing toward the axis and a gentle dipping volcanic slope facing away. We suggest that these hills are remnants of old split axial volcanic ridges that have been transported onto the flanks and that they result from successive periods of magmatic construction and tectonic dismemberment, i.e., a magmato-tectonic cycle. We observe that large abyssal hills are in ridge sections of thicker crust, whereas smaller abyssal hills are in ridge sections of thinner crust. This suggests that the magma supply controls the size of abyssal hills. The abyssal hills in ridge sections of thinner crust are regularly spaced, indicating that the magmato-tectonic cycle is a pseudoperiodic process that lasts ~0.4 m.y., about 4 to 6 times shorter than in ridge sections of thicker crust. We suggest that the regularity of the abyssal hills pattern is related to the persistence of a nearly constant magma supply beneath long-lived segments. By contrast, when magma supply strongly decreases and becomes highly discontinuous, regular abyssal hills patterns are no longer observed.

Components: 8708 words, 11 figures, 3 tables.

Keywords: side scan sonar; abyssal hills; Southwest Indian Ridge; axial volcanic ridge; magmato-tectonic cycle.

Index Terms: 3035 Marine Geology and Geophysics: Midocean ridge processes; 3045 Marine Geology and Geophysics: Seafloor morphology and bottom photography; 9340 Information Related to Geographic Region: Indian Ocean; 1550 Geomagnetism and Paleomagnetism: Spatial variations attributed to seafloor spreading (3005); 8122 Tectonophysics: Dynamics, gravity and tectonics.

Received 30 July 2002; **Revised** 20 February 2003; **Accepted** 16 March 2003; **Published** 10 May 2003.

Mendel, V., D. Sauter, C. Rommevaux-Jestin, P. Patriat, F. Lefebvre, and L. M. Parson, Magmato-tectonic cyclicity at the ultra-slow spreading Southwest Indian Ridge: Evidence from variations of axial volcanic ridge morphology and abyssal hills pattern, *Geochem. Geophys. Geosyst.*, *4*(5), 9102, doi:10.1029/2002GC000417, 2003.

Theme: Accretionary Process Along the Ultra-Slow Spreading Southwest Indian Ridge
Guest Editors: Catherine Mevel and Daniel Sauter

1. Introduction

[2] Abyssal hills are the main topographic features characterizing the ocean floor. They are present on the flanks of all mid-ocean ridges. The origin of these hills, parallel to isochrons, has been a subject of debate for over 40 years. Models proposed for their formation conflict over whether the abyssal hills are created on the spreading axis or at some distance off-axis and whether these hills owe their relief and shape primarily to volcanic constructional processes, faulting, or some combination of the two. Models of lithospheric stretching at mid-ocean ridges show that changes in the pattern of faulting occur spontaneously during stretching of a brittle layer suggesting the possibility that the kind of fault pattern that may produce abyssal hill topography need not depend on magmatic supply variations [*Poliakov and Buck*, 1998; *Buck and Poliakov*, 1998]. By contrast, magmato-tectonic cycle models suggest that the formation of abyssal hills results from the interplay of volcanic constructional processes and normal faulting that occur at or near the ridge axis [e.g., *Parson et al.*, 1993; *MacDonald et al.*, 1996]. Massifs are magmatically built within the axial valley, then split during an amagmatic period when tectonic processes predominate, and are transported onto the flanks, with little or no deformation [*Kappel and Ryan*, 1986; *Pezard et al.*, 1992]. The distribution of abyssal hills, observed on the flanks of slow to fast spreading ridges, has been interpreted as the result of alternating periods of on-axis magmatic and amagmatic activity [e.g., *Malinverno and Pockalny*, 1990].

[3] At slower spreading rates (<20 km/m.y.), theoretical models such as that by *Bown and White* [1994] predict a reduction of crustal thickness from enhanced conductive cooling. Restricted melting under the ultra-slow spreading Southwest Indian Ridge (SWIR) have indeed been suggested by both geochemical data [*Robinson et al.*, 1996] and seismic measurements [*Muller et al.*, 1999]. Some models linking crustal thickness to spreading rate become unstable at spreading rates <20 km/m.y. possibly as a consequence of the breakdown in steady state conditions. For example, *Sotin and Parmentier* [1989] showed temporal fluctuations in melt production for spreading rate of 20 km/m.y. *Louden et al.* [1996] also suggested that for ultra-slow spreading ridges the rate of such pulse of melt production does not keep pace with the rate of plate separation leading to a crustal thinning. However, until now there were only sparse data at ultra-slow spreading ridges to test the occurrence of pulses in magmatic activity and to analyze their possible contribution to the off-axis morphology.

[4] We use here both on-axis and off-axis geophysical data of the SWIR to document the along-axis variability of volcanic ridges and to provide new insights into their evolution through time on the flanks of the ridge. First, we use the fine-scale side scan sonar data collected within the SWIR axial valley during the French-UK-Japanese InterRidge (FUJI) cruise (R/V Marion Dufresne, October 1997) [*Tamaki et al.*, 1998; *Sauter et al.*, 2002a]. We present the distribution of volcanic and tectonic features along the axial valley. We interpret differences in volcanic and tectonic morphologies as stages in an evolutionary life cycle of axial volcanic ridge development. Off-axis bathymetric, gravimetric and magnetic data collected during the Gallieni cruise (R/V L'Atalante, October 1995) [*Patriat et al.*, 1996] allow us to determine the size, shape and distribution of the abyssal hills that we interpret as remnants of axial volcanic ridges. We suggest that periods of volcanic construction alternate with peri-

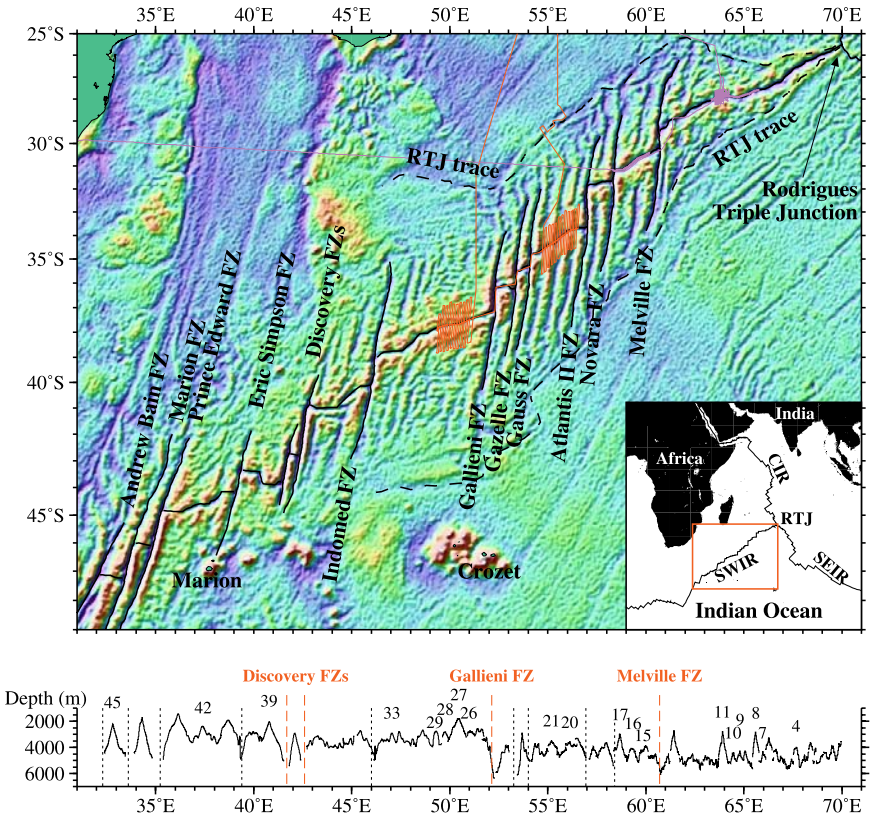

Figure 1. Structural map (top) and along-axis bathymetric profile (bottom) of the Southwest Indian Ridge (SWIR) between 31°E and 70°E. On the structural map, thick black lines indicate the fractures zones, the triple junction traces and the SWIR axis which are interpreted from the free air gravity anomalies (shown in background) derived from satellite sea-surface altimeter measurements [*Smith and Sandwell*, 1995]. Tracks of the FUJI cruise are shown by magenta lines. Tracks of the Gallieni cruise are shown by red lines. SEIR: Southeast Indian Ridge; CIR: Central Indian Ridge; RTJ: Rodrigues Triple Junction. On the bathymetric profile, the segments cited in the text and/or in other figures are identified by their number, following the nomenclature of *Cannat et al.* [1999]. Along-axis bathymetric data were collected during the Capsing cruise (R/V L'Atalante, 1993; 57–70°E) [*Patriat et al.*, 1997], the Gallieni cruise (49–57°E) and the SWIFT cruise (R/V Marion Dufresne, 2001; 32–49°E) [*Humler et al.*, 2001]. The Discovery, Gallieni and Melville FZs bound three major SWIR sections (see text for further details).

ods of tectonic dismemberment to built the abyssal hills. We propose that the size of these abyssal hills is related to the magma budget beneath the segments and that their succession is related to the persistence of the magma supply.

2. Regional Setting

[5] The SWIR is a major plate boundary separating Africa and Antarctica with an ultra-slow spreading rate of about 16 km/m.y. [*DeMets et al.*, 1990]. From the Andrew Bain fracture zone (FZ; 32°E) to the Rodrigues triple junction (70°E), this spreading rate is almost constant [*Patriat et al.*, 1997] whereas the spreading direction evolves eastward from N18°E to N0°E. Many characteristics vary along-axis, including the mean axial depths, the obliquity of the ridge axis (with respect to the normal to the spreading direction), the present-day small-scale segmentation and the presence or absence of long-lived transform and non-transform discontinuities. Major changes occur across the Discovery (42°E), Gallieni (52°20′E) and Melville (60°45′E) FZs defining the large-scale segmentation of the SWIR. Mean axial depths (Figure 1) decrease eastward from 3050 m, between the Andrew Bain and Discovery FZs, to 3530 m between the Discovery FZ and ~49°30′E, and then

increase to 3090 m in a short section, between ~49°30′E and the Gallieni FZ [*Humler et al.*, 2001; *Sauter et al.*, 2002b]. They decrease again from 4330 m between the Gallieni and Melville FZs to 4730 m in the deepest part of the ridge, between the Melville FZ and the Rodrigues triple junction [*Cannat et al.*, 1999]. This large-scale variation of axial depths suggests that the regional density structure of the axial region also varies. The shallowest ridge section, west of the Discovery FZ, probably correspond to the region affected by the Marion hot spot [*Georgen et al.*, 2001] whereas the deepest ridge section to the east of the Melville FZ is thought to be underlain by thin crust and/or cold mantle [*Cannat et al.*, 1999; *Meyzen et al.*, 2003]. To the west of ~49°30′E, the ridge has an overall obliquity of ~40° and is characterized by several long-lived discontinuities (Figure 1). The short shallow section between ~49°30′E and the Gallieni FZ has an overall obliquity of 20° and is devoid of such long-lived discontinuities (Figure 1). Between the Gallieni and Melville FZs the ridge has an overall obliquity of 45° and is characterized by many long-lived discontinuities (Figure 1). By contrast, the ridge section east of the Melville FZ has an overall obliquity of 25° and is devoid of such long-lived discontinuities (Figure 1). The along-axis depth profile, between the Gallieni and Melville FZs, displays relatively homogeneous segment lengths (~40 km) and along-axis relief (~1000 m) but with large non-transform discontinuities (NTDs). By contrast, to the east of the Melville FZ, the segmentation is highly variable with three major segments with along-axis relief up to 2600 m, spaced every ~200 km, and segments with significantly less relief (<1000 m) in between.

3. Along-Axis Variability of Volcanic Ridges

3.1. Geology of the SWIR Axial Valley From TOBI Imagery

[6] During the FUJI cruise, TOBI (Towed Ocean Bottom Instrument) [*Flewellen et al.*, 1993] side scan sonar images of the SWIR axial valley floor were acquired on the deepest section of the SWIR underlain by cold mantle, to the east of the Melville FZ, and on the shallower oblique section to the west of the Melville FZ (Figure 1). TOBI was operated at altitudes of 250–700 m above the seafloor with a tow speed of about 2 knots along two parallel tracks spaced at approximately 5 km. This resulted in two mosaics of imagery about 190 km long and 11 km wide from 58°30′E to 60°12′E and 230 km long and 11 km wide from 63°23′E to 65°45′E (Figure 2). The final horizontal resolution of the gridded data is 6 m. This type of TOBI mosaic covers almost the entire inner valley floor at segment centers but neither the walls of the axial valley nor the edges of the largest NTDs were ensonified continuously (Figure 2).

[7] The TOBI images allow us to differentiate areas covered with volcanic constructions from areas devoid of such features showing advanced tectonic dismemberment. Seven segments were imaged during the survey, three to the west of the Melville FZ (segments 15, 16 and 17 in the nomenclature of *Cannat et al.* [1999]) and four to the east of the Melville FZ (segments 8, 9, 10 and 11) (Figure 2). As in previous works using deep-towed side scan sonar imagery [*Smith et al.*, 1995; *Gràcia et al.*, 1998; *Briais et al.*, 2000; *Sauter et al.*, 2002a], we have distinguished three main types of volcanic constructions: flat-topped volcanoes, hummocky terrains and smooth lava flows. Hummocky terrains are by far the most widespread. They consist in numerous small (<500 m diameter) rounded mounds which are either irregularly aggregated or less frequently aligned along trends striking mostly E-W. Uniformly highly reflective areas are interpreted as smooth lava flows. Few large-scale flat-topped volcanoes were observed in the survey area. These different volcanic features are often cut by linear, narrow reflectors that are inferred to be fault scarps. Elsewhere, large regions of high reflectivity are interpreted as landslide zones, generally associated with axial valley walls. In addition to these volcanic and tectonic features, large areas with uniformly low backscatter are inferred to be covered by sediments.

[8] Volcanic terrains within the seven segments surveyed show various degrees of deformation: from relatively recent volcanic areas with almost no fractures and/or fissures to totally dismembered

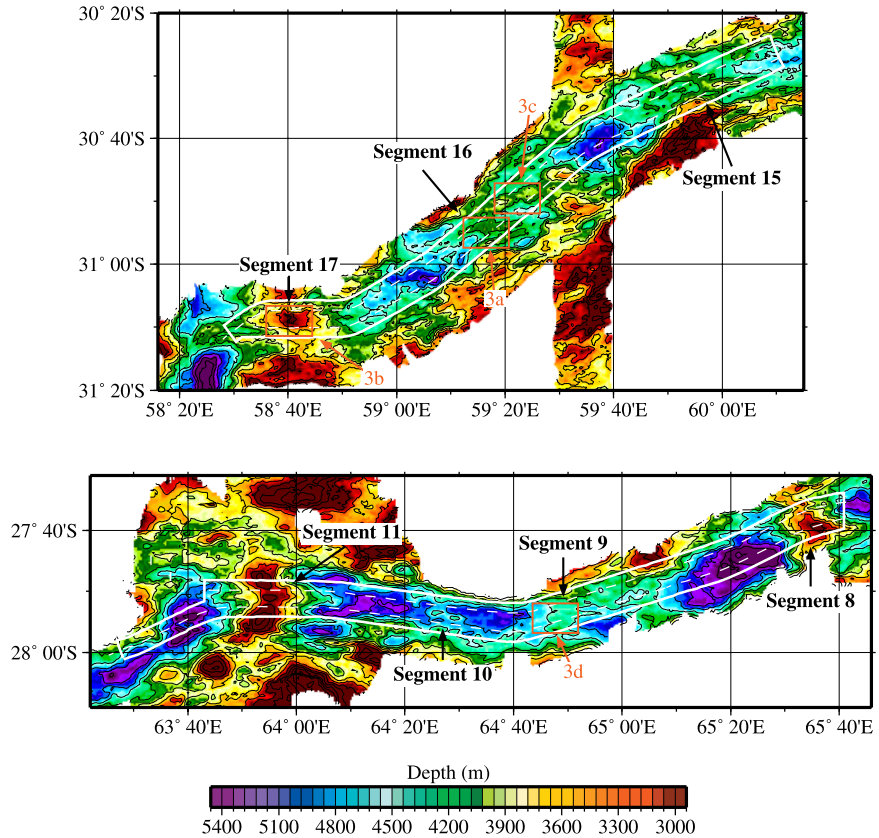

Figure 2. Bathymetric maps of the Southwest Indian Ridge (SWIR) from 58°16′E to 60°15′E (top) and from 63°22′E to 65°46′E (bottom). Color interval is every 60 m. Contour interval is every 300 m. The multibeam bathymetric data were collected during the Capsing cruise (R/V L'Atalante, 1993), the FUJI cruise (R/V Marion Dufresne, 1997) and the Kerimis cruise (R/V Marion Dufresne, 1998). Segments are identified by their number. Dashed white lines indicate the TOBI tracks. Thick white lines bound the TOBI imagery. Small red squares indicate the location of the TOBI images presented in Figures 3a–3d.

zones with very intense faulting and fissuring. We have distinguished three main types of axial ridges according to these degrees of deformation. The first type corresponds to axial volcanic ridges (AVRs) where highly reflective volcanic features and few faults or fissures are observed. This is the case for segment 11 (Jourdanne mountains), segment 15 and the western axial ridge of segment 16. The E-W trending AVR of segment 11 (centered at 63°55′E) is 47 km long, 6 km wide (at the segment center) and is associated with a large accumulation of volcanic material, hummocks as well as smooth lava flows, that dominates the entire axial valley at the segment center. In contrast, the 35 km long and 6 km wide western axial ridge of segment 16 (centered at 59°20′E) lies within a deep large axial valley. This sigmoid-shaped ridge is about 500 m high and is associated with highly reflective and dense hummocky terrain (Figure 3a). A 1.5 km diameter flat-topped volcano is located on top of this ridge (Figure 3a). Segment 15 (centered at 59°54′E) includes several fresh-looking hummocky ridges with various strikes. The small hummocky ridges located in the western part of the segment are 1.5–2 km wide, 200 m high and 3 km long while, to the east, the main axial ridge is wider (5 km), higher (600 m), longer (up to 20 km) and strikes E-W.

[9] The second type of axial ridge corresponds to partially faulted volcanic constructions, cut by faults and fissures. This is the case for segments 17, 10 and 8 (centered at 58°40′E, 64°27′E and 65°36′E respectively). The 9 km wide, 41 km long, 800 m high AVR of segment 17 is an E-W trending

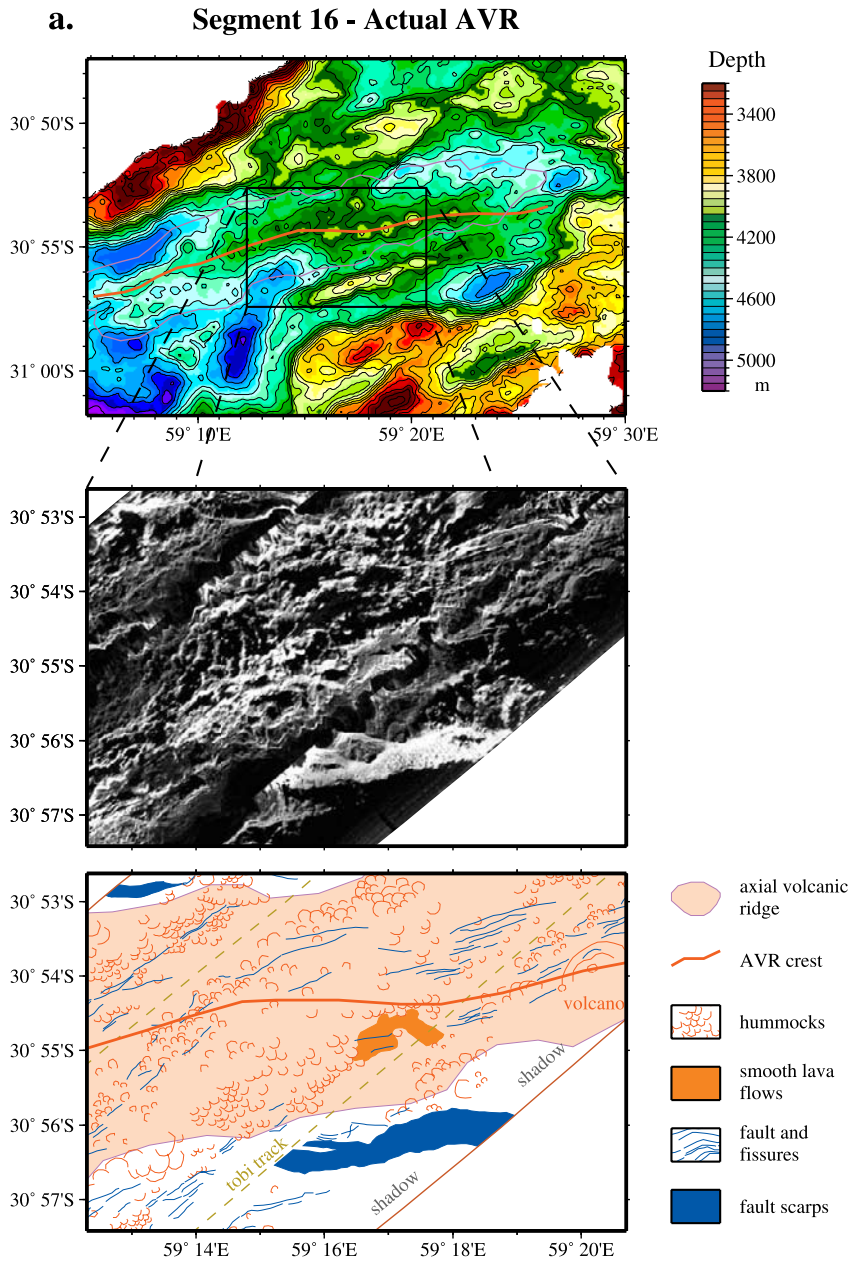

Figure 3. Bathymetric maps, TOBI side scan sonar images and their geological interpretation showing examples of the three main types of axial ridges identified in this study. (a) The fresh-looking axial volcanic ridge of segment 16 (actual AVR). (b) The partially faulted axial volcanic ridge of segment 17. (c) The tectonized axial ridge of segment 9. (d) The tectonized axial ridge of segment 16 (earlier AVR). On the bathymetric maps, thick black lines bound the TOBI imagery, magenta lines limit the axial volcanic ridges and thick red lines correspond to the summit of the ridge. White is high reflectivity and dark is low reflectivity in the TOBI images.

broad heterogeneous pile of fresh-looking and faulted hummocks. Its southern flank shows a fine-scale faulted texture locally overprinted by isolated hummocks and hummocky ridges. Deformation is less distributed on its northern flank where areas of hummocky terrain are cut by major fault scarps (Figure 3b). The small graben (5 km long, 0.7 km wide, 80 m deep) located on top of the AVR and observed on the bathymetric map has not been ensonified by the TOBI. The AVR of segment 8 (9 km wide, 40 km long and 1000 m high) has similar characteristics, with hummocky

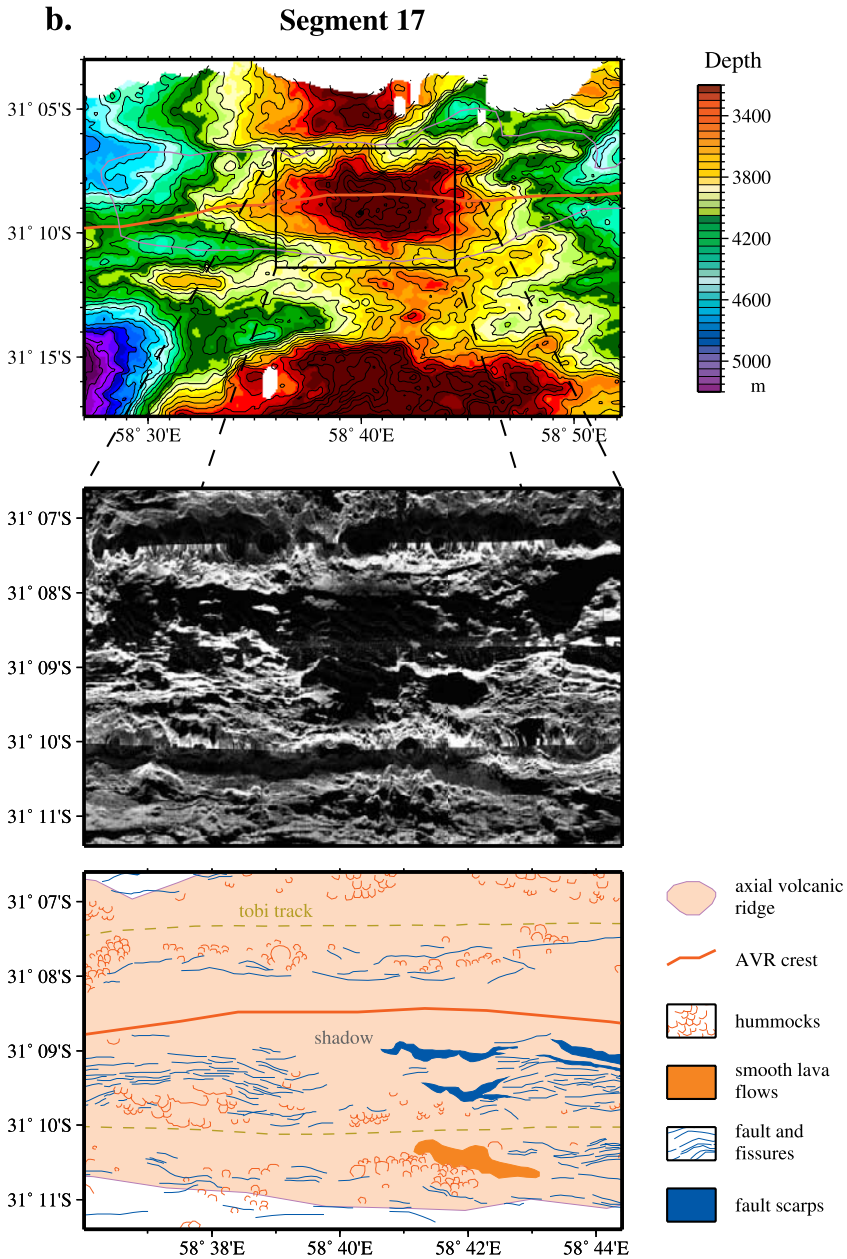

Figure 3. (continued)

terrain cut by large faults on its northern flank and fine-scale faulted smooth lava surfaces on its southern flank. Segment 10 includes two E-W trending AVRs in an en echelon array. These 8 km long, 4.5 km wide and 400–500 m high AVRs are associated with hummocky terrains cut by long E-W trending major fault scarps.

[10] The third type of axial ridge corresponds to central ridge systems with no intact volcanic features which instead are dominated by a series of closely spaced faults and fissures. This is the case for the 26 km long, 15 km wide segment 9 (centered at 64°49′E) where both the axial valley floor and the 300 m high ridge appear to be totally dismembered by both small-scale intense faulting and major fault scarps (Figure 3c). Similarly, the eastern axial ridge of segment 16 is a 23 km long, 8 km wide, 450 m high, N80°E-striking tectonized ridge which is surrounded by fresh-looking hum-

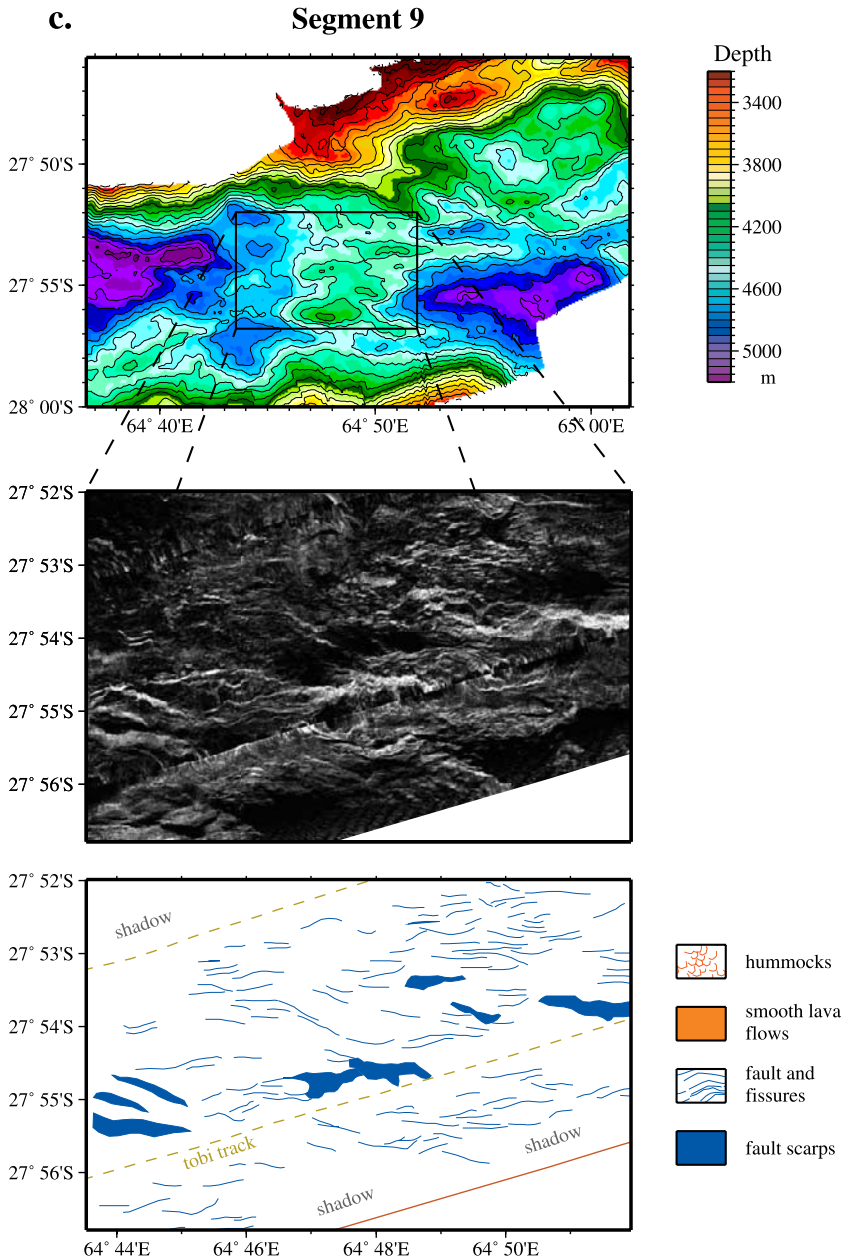

Figure 3. (continued)

mocky terrain (Figure 3d). Hummocky texture could only be identified within an area of low backscattering at the eastern extremity of this tectonized ridge, although basalts have been dredged in its central part [*Mével et al.*, 1997]. The dimensions, orientation and location of this ridge at the shallowest part of the segment 16 suggest that it could represent an early dismembered AVR. Fresh-looking and partially faulted axial volcanic ridges have been observed on the MAR and the Reykjanes ridge [*Briais et al.*, 2000; *Parson et al.*, 1993], but totally dismembered axial ridges have never been observed on slow spreading ridges.

3.2. Along-Axis Variations of Axial Valley Morphology

[11] As only a few segments have been covered by TOBI imagery, we have used along-axis multi-

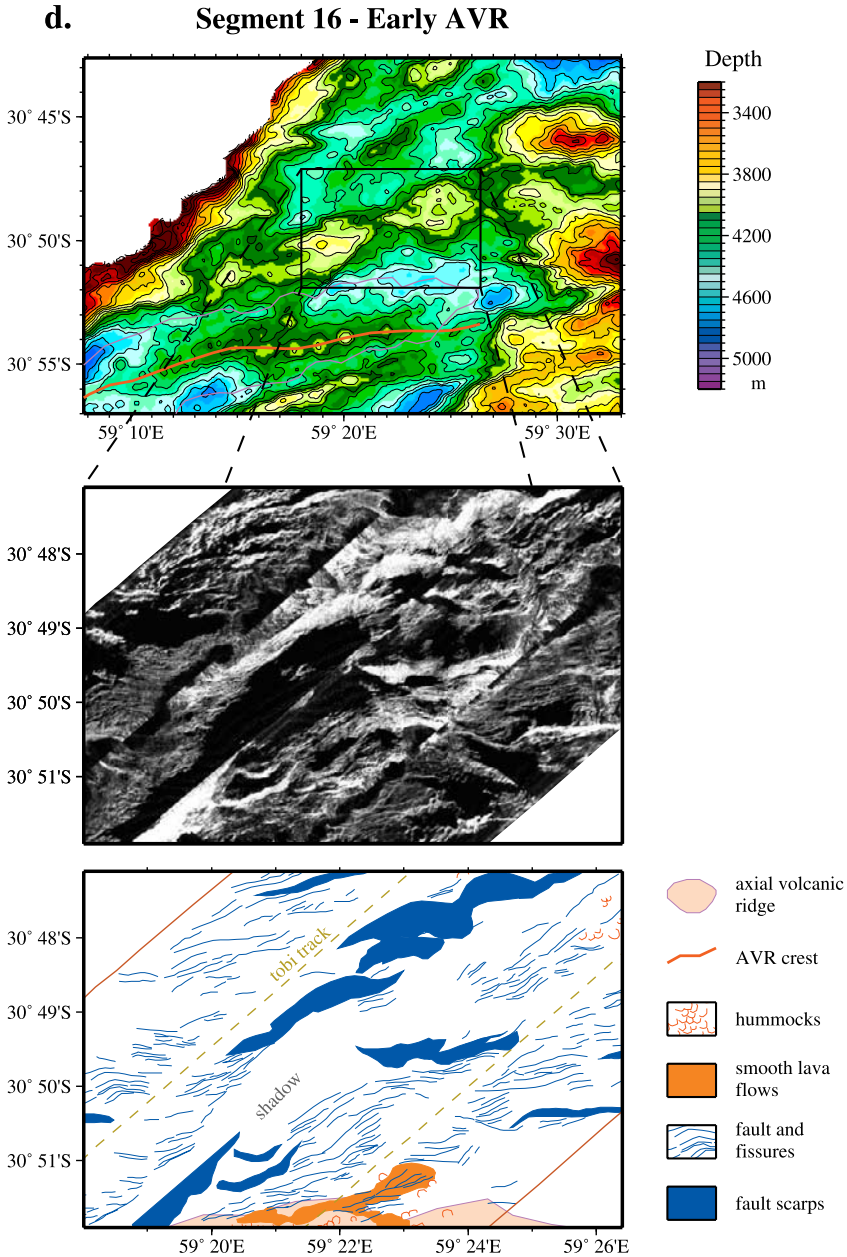

Figure 3. (continued)

beam bathymetric data, from 32°E to 70°E, to analyze the axial ridges of 45 SWIR segments. Figure 4 shows that the length of these axial ridges tends to increase with increasing height of the ridges suggesting that they may lengthen and grow as they become more mature. The evolution of the height of axial ridges is illustrated in Figure 5 which presents a selection of cross sections over different SWIR segment centers. The shape of the axial valley varies from a deep graben with no axial ridge (segment 20) to a valley entirely filled (segment 27) by volcanic material indicated by numerous conical seamounts. Between these two extremes, the height of the axial ridge lying on the axial valley floor increases from 100 m (segment 7) to 800 m (segment 17). For the last four examples (segments 39, 11, 45 and 27), the axial valley is partly (segments 39 and 11) to entirely filled (segments 45 and 27) and axial ridges are barely recognizable at segment centers. TOBI imagery

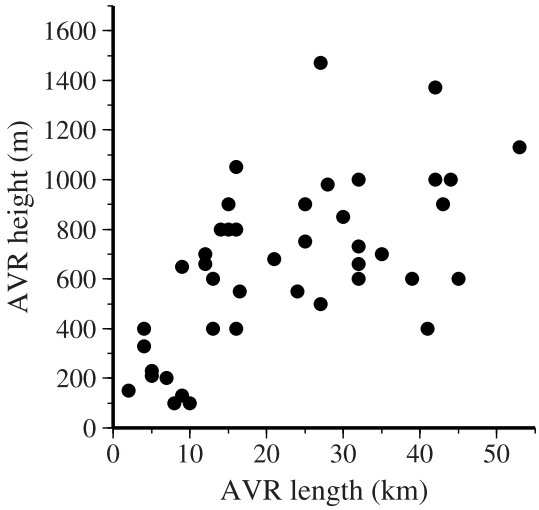

Figure 4. Height versus length of axial volcanic ridges of SWIR segments located between 32°E and 70°E. Bathymetric data were collected during the Capsing cruise (57–70°E) [*Mendel et al.*, 1997], the Gallieni cruise (49–57°E), the SWIFT cruise (35–49°E) [*Humler et al.*, 2001] and the KN145L16 cruise (west of 35°E) [*Grindlay et al.*, 1996].

and cross sections show that fresh looking volcanic constructions are observed on small ridges (segment 15) as well as on larger ones (segment 16) and in sections of the ridge where the axial valley is partly filled (segment 11). Likewise, partially faulted volcanic constructions are observed on small AVRs (segment 10) as well as on larger ones (segment 17) indicating that AVRs may reach different sizes before being cut by faults.

4. Variability of Abyssal Hills on the Flanks of the SWIR

[12] During the Gallieni cruise, multibeam bathymetric data, as well as magnetic and gravimetric data, were acquired out to 12 m.y. old crust in two survey areas (Figure 1). The western off-axis survey area is located in the short shallow SWIR section between 49°30′E and the Gallieni FZ. Like the western TOBI survey area, the eastern off-axis survey area, from 54°35′E to the Atlantis II FZ, is located in the oblique SWIR section between Gallieni and Melville FZs. In both off-axis survey areas, the axial valley and flanks are fully covered using ~200 km long profiles parallel to the spreading direction and spaced approximately 7 km apart. Using the magnetic profiles, we have picked the magnetic anomalies 1 (0.78 Ma), 3a (5.894 Ma) and 5 (10.949 Ma) for the western off-axis survey area and the magnetic anomalies 1, 2a (2.581 Ma), 3a, 4a (8.699 Ma) and 5 for the eastern off-axis survey area (geomagnetic reversal timescale of *Cande and Kent* [1995]). The mag-

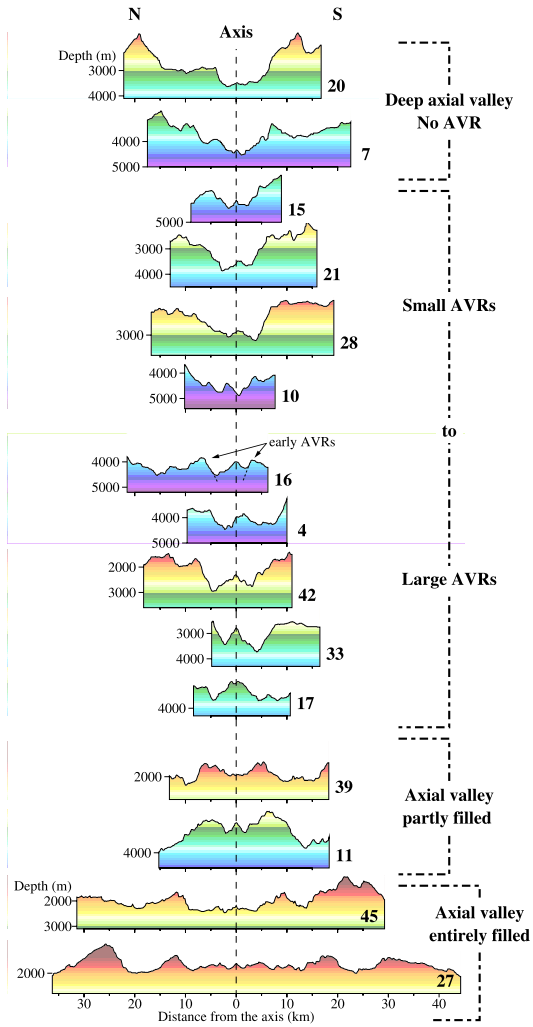

Figure 5. Bathymetric cross sections of segment centers classified as a function of the axial valley morphology: from a deep axial valley with no AVR (top) to an axial valley entirely filled (bottom). Segments are identified by their number, following the nomenclature of *Cannat et al.* [1999] (see Figure 1 for location). For segments 33, 39, 42 and 45, bathymetric data were collected during the KN145L16 cruise [*Grindlay et al.*, 1996] and the SWIFT cruise [*Humler et al.*, 2001].

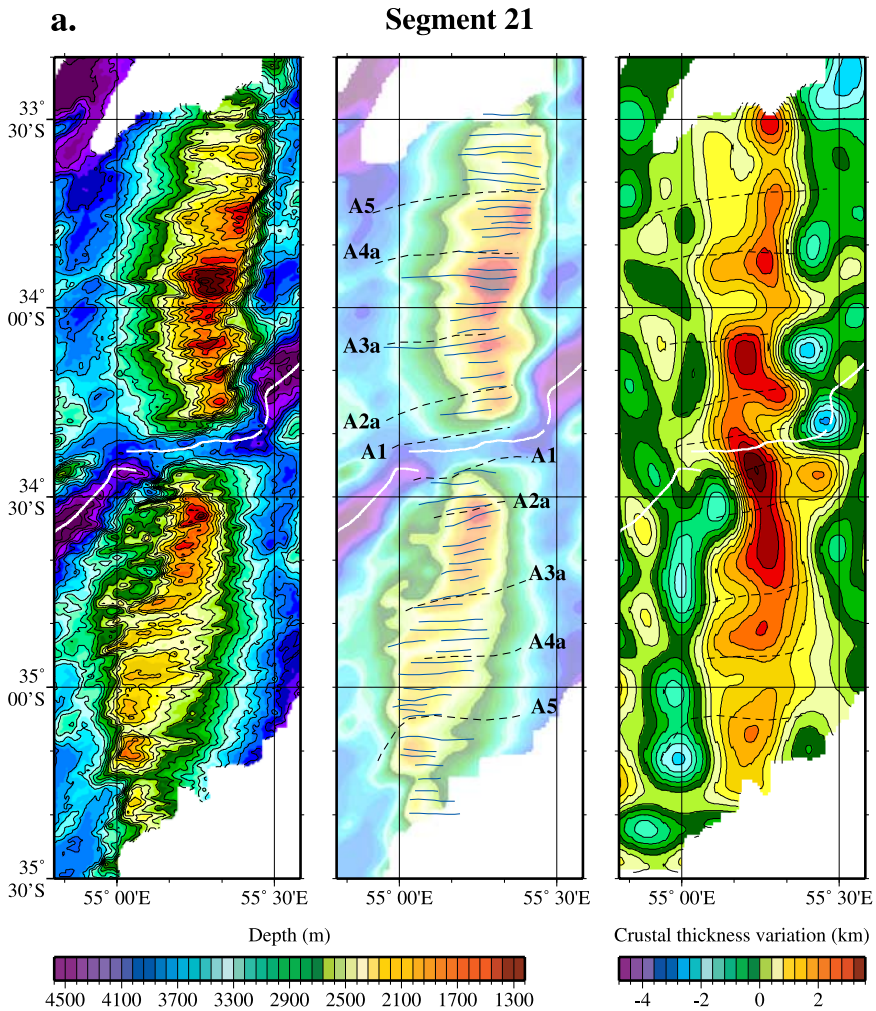

Figure 6. Bathymetric, structural interpretation and crustal thickness variation maps of the SWIR over segments 21 (a) and 20 (b), out to the 12 Ma isochron. Crustal thickness variation maps are deduced from residual gravity anomaly following *Rommevaux et al.* [1994]. On the structural maps, with smoothed bathymetry in the background, blue lines indicate the top of the abyssal hills. Thick white lines indicate the axis. Dashed black lines indicate the isochrons (A: anomaly). A1 = 0.78 Ma, A2a = 2.581 Ma, A3a = 5.894 Ma, A4a = 8.699 Ma and A5 = 10.949 Ma (geomagnetic reversal timescale of *Cande and Kent* [1995]).

netic structure of these survey areas will be published elsewhere (D. Sauter et al., manuscript in preparation, 2003).

4.1. Off-Axis Survey Area Between 54°35′E and the Atlantis II FZ

[13] The present-day segmentation of this survey area consists of two N80-90°E striking segments (20 and 21 in the nomenclature of *Cannat et al.* [1999]) limited by two oblique NTDs (west and east of segment 21) and the Atlantis II FZ (east of segment 20). The large NTD which separates the two segments offsets the axis by 65 km. Segments 20 (centered at 56°08′E) and 21 (centered at 55°12′E) correspond to 900–1300 m high along-axis reliefs (40–45 km long) (Figure 6). The 30 km long axial ridge associated with segment 21 is 150 m high (measured across-axis at the segment center) while there is no axial ridge associated with segment 20. The segmentation is easy to follow off-axis. The off-axis traces of the segments correspond to large block mountains (1800–2700 m high) with a general orientation of N03–06°E, parallel to the spreading direction (Figure 6). These block mountains are bordered by depressions cor-

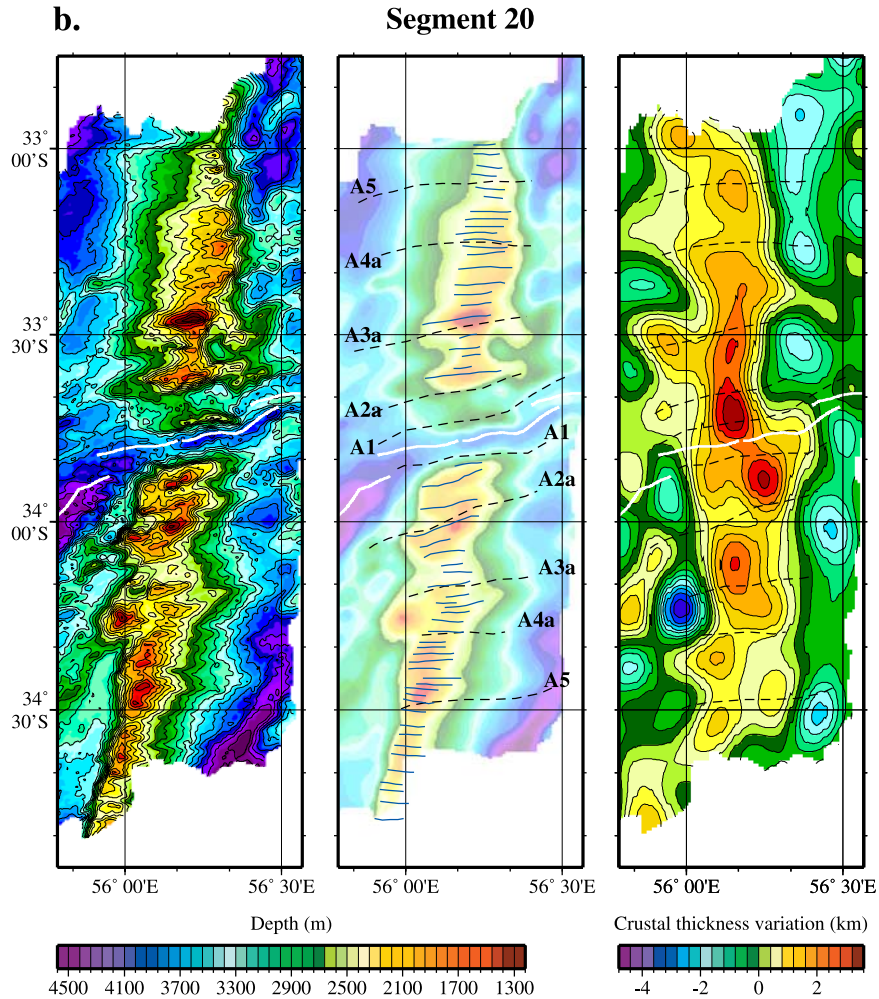

Figure 6. (continued)

responding to the NTDs off-axis traces. On the crustal thickness anomaly maps, the block mountains and adjacent NTDs correspond to areas of thicker and thinner crust, respectively (Figure 6). Magnetic anomalies identified over these block mountains show that spreading has been asymmetric during different periods of time for segments 20 and 21 (Table 1).

Table 1. SWIR Spreading Rate for Segments 20 and 21

	A1–A2a	A2a–A3a	A3a–A4a	A4a–A5	A1–A5
			Segment 20		
Half-spreading rate, km/m.y.					
North flank	4.95	5.81	8.71	8.00	6.94
South flank	8.36	6.21	4.98	8.83	6.83
Asymmetry, %	−25.6	−3.3	27.2	−4.9	0.8
Full-spreading rate, km/m.y.	13.31	12.02	13.69	16.83	13.77
			Segment 21		
Half-spreading rate, km/m.y.					
North flank	6.61	4.94	8.32	8.13	6.87
South flank	6.75	7.45	6.18	7.59	7.01
Asymmetry, %	−1.0	−20.3	14.8	3.4	−1.0
Full-spreading rate, km/m.y.	13.36	12.39	14.50	15.72	13.88

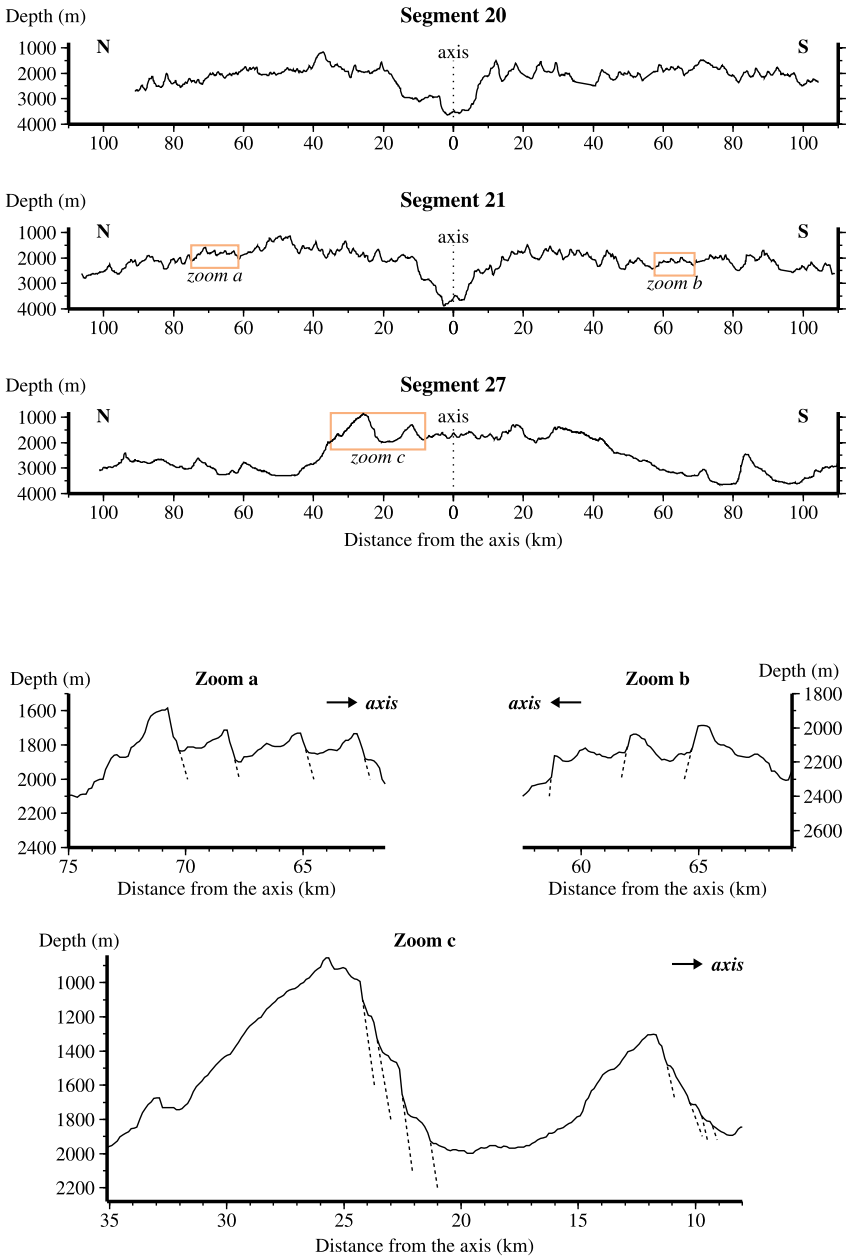

Figure 7. Bathymetric cross sections (parallel to the spreading direction) of abyssal hills of segment 20, 21 and segment 27, with enlargements on small portions of them.

[14] Superimposed on the block mountains, abyssal hills form elongated ridges, perpendicular to the spreading direction (Figure 6). They are 3 km wide on average (measured in the spreading direction) and 100–350 m high (160 m high on average). The height of the abyssal hills decreases toward the NTDs traces where they disappear. Their lengths vary between 15 and 45 km. These hills are mostly asymmetric, with a steep slope facing toward the axis and a gentle slope facing away (Figure 7). The outward-facing slopes are generally characterized by lobate features and sometimes crowned by conical seamounts. These abyssal hills, with similar dimensions (height, length and width) to the AVR of segment 21, are thus interpreted as remnants of old axial volcanic ridges. The mean distances between successive abyssal hills are about the same on each flank of the two segments

Table 2. Abyssal Hills Spacing

	Number of Abyssal Hills	Distance, m	Half-Spreading Rate, km/m.y.	Time Interval, m.y.
		Segment 20		
North flank	23	3063.20 ± 1014.60	6.94	0.441 ± 0.146
South flank	35	3037.54 ± 1277.55	6.83	0.445 ± 0.187
		Segment 21		
North flank	28	2995.22 ± 722.98	6.87	0.435 ± 0.105
South flank	32	3199.94 ± 931.33	7.01	0.456 ± 0.133
		Both Segments		
Both flanks	118	3076.97 ± 1035.56	6.91	0.445 ± 0.150

(Table 2). Using these distances and the mean half-spreading rate measured between anomalies 1 and 5 (i.e., 6.91 km/m.y.), we obtained a 0.445 m.y. mean span of time between successive abyssal hills with a standard deviation of 0.150 m.y. This indicates a pseudoperiodic process resulting in the formation of successive abyssal hills with similar sizes on both segments over the last 12 m.y.

[15] Aside from the small-scale topographic variations, we observe, along the block mountains, a strong larger-scale variation in bathymetry and crustal thickness anomaly (Figure 6). Areas of relatively thicker crust are about 20–30 km wide (measured across axis) and are either circular or elongated parallel to the spreading direction. The mean peak-to-trough amplitude in crustal thickness is 0.8 km (Figure 8). We observe large topographic swells 600–900 m high and 20–45 km wide (measured in the spreading direction), with abyssal hills superimposed (Figure 6), which correspond more or less to areas of relatively thicker crust. The across-axis variations of crustal thickness have relatively consistent wavelength, and suggest reg-

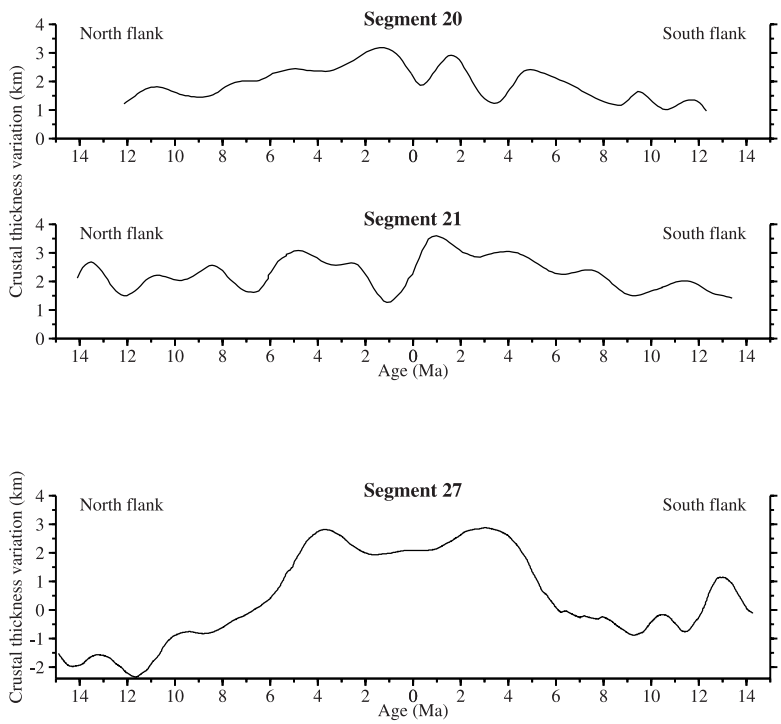

Figure 8. Crustal thickness variation profiles (parallel to the spreading direction) at segments 20, 21 and 27.

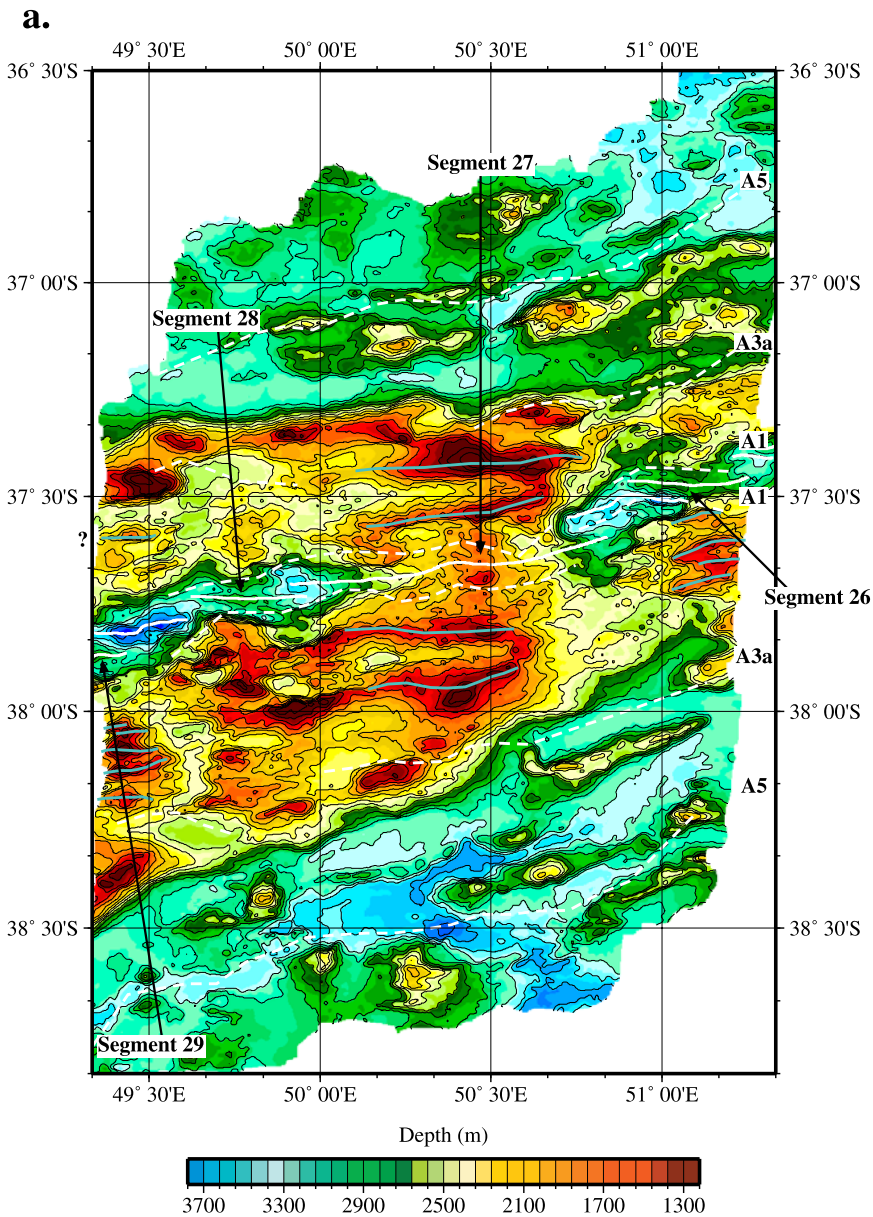

Figure 9. (a) Bathymetric map and (b) crustal thickness variation map of the western off-axis survey area, out to the 12 Ma isochron. Cyan lines indicate the top of the abyssal hills. Thick white lines indicate the axis. Dashed white lines indicate the isochrons (A: anomaly). A1 = 0.78 Ma, A3a = 5.894 Ma and A5 = 10.949 Ma (geomagnetic reversal timescale of *Cande and Kent* [1995]).

ular changes in magma supply every ~3 m.y. (Figure 8). These variations, as well as the large and small-scale topographic variations, are not synchronous at segment 20 and segment 21 (Figure 8). This non-synchronization is also observed in spreading asymmetry: for example, during the anomaly 2a–3a period, segment 21 is spreading asymmetrically while segment 20 is spreading symmetrically (Table 1). Thus, although segments 20 and 21 have a similar evolution (similar abyssal hill sizes and periodicity, and similar crustal thickness variations), the non-synchronization suggests that segments 20 and 21 evolve independently.

4.2. Off-Axis Survey Area West of the Gallieni FZ

[16] The present-day segmentation of this survey area consists of four segments (26, 27, 28 and the

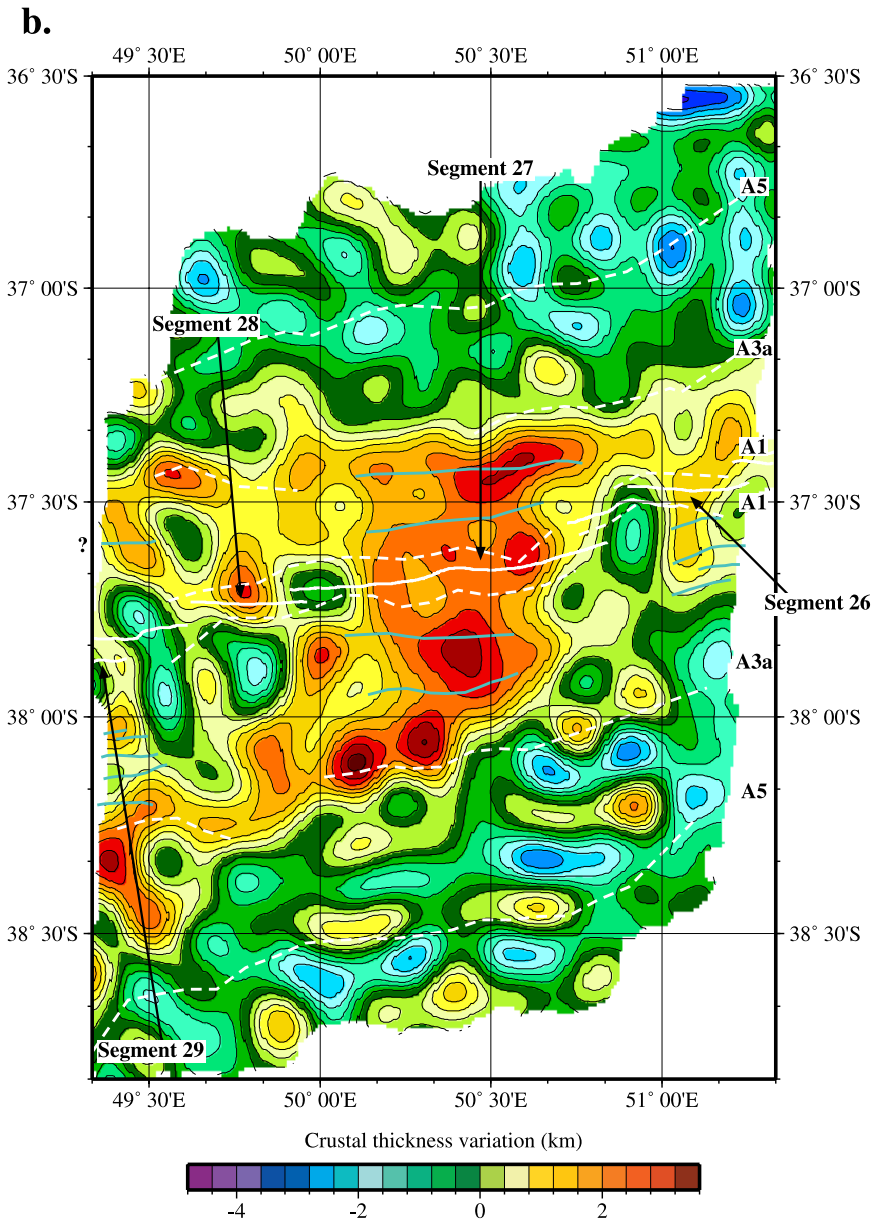

Figure 9. (continued)

eastern end of segment 29) limited by four NTDs [*Sauter et al.*, 2001]. This slightly oblique section of the SWIR is characterized by the absence of an axial valley in its shallowest region (<1600 m) centered at 50°28′E. The axial valley free region corresponds to the central part of segment 27 (Figure 9a), a 85 km long feature of high relief (1900 m measured along- axis). Segments 26 and 28, centered at 51°07′E and 49°45′E, respectively, are shorter and with less relief (40 km long and 650 m high). On each side of segment 27, NTDs offset the axis by 18 km and 10 km. The most striking features on the flanks are two large outward facing scarps, located at 40–70 km from the axis, which bound a central axial domain 1000–1500 m shallower than the older lithosphere (Figure 9a). This shallow domain corresponds to an area of 2–3 km thicker crust than the older deeper lithosphere (Figure 9b). Its V-shape, pointing toward the east, observed both in the bathymetric

Table 3. SWIR Spreading Rate for Western Off-Axis Survey Area

	Half-Spreading Rate, km/m.y.			
	North Flank	South Flank	Asymmetry, %	Full-Spreading Rate, km/m.y.
		Segment 27		
A1–A3a	5.87	8.02	−15.5	13.89
		Total Area[a]		
A1–A3a	5.2	8.7	−25.2	13.9
A3a–A5	7.0	8.0	−6.7	15.0

[a] Because the segmentation is unstable, except for segment 27 until A3a, we calculated mean spreading rates over the total area.

and crustal thickness maps, suggests the propagation of a melting anomaly.

[17] In contrast to the eastern off-axis survey area, this ridge section has no clear off-axis segmentation except for segment 27 for which we can follow its off-axis traces until the edges of the central domain (Figure 9a). These off-axis traces are characterized by four large E-W elongated domes which are about 60 km long and 500–900 m high (Figure 9a). The width of these domes (10–22 km) decreases toward their terminations forming a bow-shaped structure in plan view (Figure 9a). These domes are asymmetric with a steep axial-facing slope, cut by a series of faults, and a gentle outward-facing slope, crowned by numerous conical seamounts (Figure 7). They thus show the same asymmetric shape as the abyssal hills of the eastern section (Figure 7) suggesting a similar formation process. The age difference between the successive domes is 2 m.y. The off-axis traces of segment 27 correspond also to a thicker crust area which is characterized by a positive anomaly at about 20 km on each side of the axis (Figure 9b). Taking into account the asymmetric spreading rate for this segment (Table 3), the widths of these anomalies (18–25 km) indicate changes in magma supply which last about 3 m.y. Peak-to-trough amplitudes in crustal thickness reach 1.2 km. The large abyssal hills are located on top of these thicker crust anomalies.

[18] On the shallow central domain, we observe two series of few small abyssal hills on the southern flank of segments 29 and 26 (centered at 49°25′E–38°10s and 51°10′E–37°40s respectively) (Figure 9a). These series are underlain by much thinner crust than beneath segment 27 (Figure 9b). Although, these small abyssal hills have no counterpart on the northern flank, they have similar size and shape to those identified on the eastern off-axis survey area. The asymmetric distribution of these hills is probably related to the high spreading rate asymmetry measured in this region (Table 3). Series of abyssal hills are no more observed on the deeper part of the flanks. Outside the central shallow domain, bathymetric highs are randomly distributed and most of them are underlain by thin crust suggesting that these features are uncompensated and that the seafloor topography is dynamically maintained. Areas of thicker crust commonly correspond to deep seafloor and are predominant in the southern deepest part of the survey area whereas they are rare in the corresponding northernmost part (Figure 9b). Such common departure from isostatic compensation of seafloor topography and pronounced asymmetry of crustal thickness and seafloor relief between the two ridge flanks have also been observed by M. Cannat et al. (Melt supply variations to a magma-poor ultra-slow spreading ridge (Southwest Indian Ridge 61° to 69°E), submitted to *Geochemistry, Geophysics, Geosystems*, 2003) (hereinafter referred to as Cannat et al., submitted manuscript, 2003) in the deepest part of the SWIR, to the east of the Melville FZ.

5. Discussion

5.1. Life Cycle of AVR Development

[19] The differences in the size and deformation of axial volcanic ridges observed in side scan sonar images suggest stages in an evolutionary life cycle

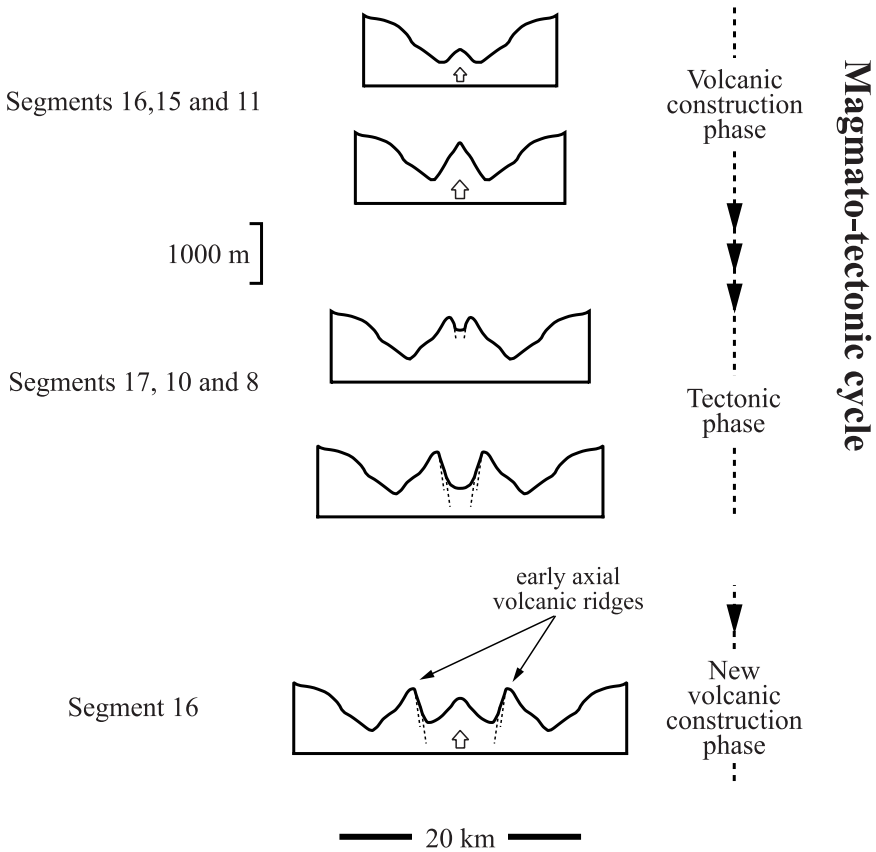

Figure 10. Magmato-tectonic cycle model showing the idealized temporal evolution of an axial volcanic ridge. The axial volcanic ridge is built during a period of volcanic construction and is split in two by normal faulting during a period of tectonic dismemberment. Normal faulting may occur either on the top of the axial volcanic ridge (as shown here) or on one flank of this ridge resulting in two abyssal hills with different sizes. The two parts are moved apart and a new axial volcanic ridge can latter form in between. In this magmato-tectonic cycle, fresh-looking axial volcanic ridges of segments 16, 15 and 11 are interpreted to be in a volcanic construction phase and partially faulted axial volcanic ridges of segments 17, 10 and 8 are interpreted to be at the beginning of a tectonic phase.

of AVR development. This cycle ranges from periods of volcanic construction, when magma supply is high enough to built volcanic ridges, to periods of tectonic dismemberment, when magma supply decreases so that tectonic extensional processes become predominant (Figure 10). According to this magmato-tectonic cycle, fresh-looking AVRs of segments 16, 15 and 11, are in a stage of volcanic construction while tectonized axial ridges, of segments 9 and 16, are in an advanced stage of tectonic dismemberment. Partially faulted AVRs (segments 8, 10 and 17) are interpreted to be in a transition period between the periods of volcanic construction and tectonic dismemberment. A rough estimation of the period of volcanic construction is obtained from the TOBI data by dividing the width of the AVRs by the SWIR mean spreading rate (16 km/m.y.). With this crude method, the fresh-looking AVRs of segments 16, 15 and 11 are 0.1–0.4 m.y. old. and the faulted AVRs of segments 17, 10 and 8 are 0.3–0.6 m.y. old. The period of volcanic construction lasts thus at least 0.3 m.y.

[20] We suggest that periods of volcanic construction alternate with periods of tectonic dismemberment to built the abyssal hills, as previously proposed for slow spreading ridges [*Pockalny et al.*, 1988]. As the abyssal hills of segments 20, 21 and 27 have similar dimensions to the AVRs observed along the SWIR axial valley, we suggest that these hills correspond to old split AVRs which have been transported onto the flanks with

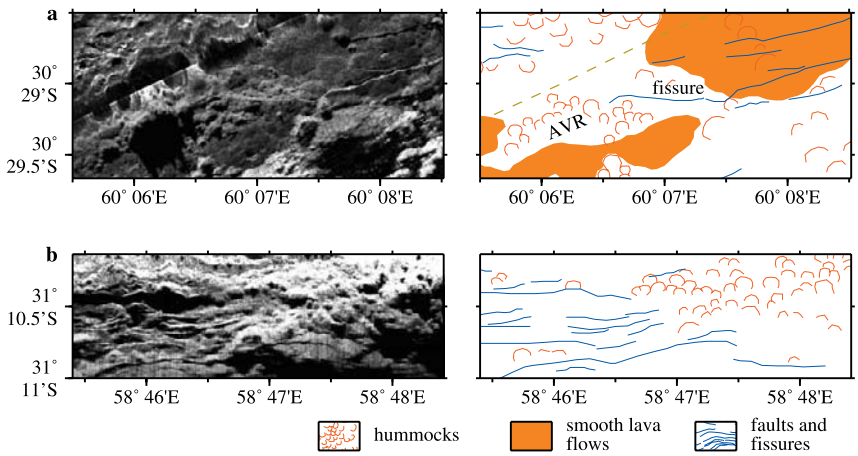

Figure 11. TOBI side scan sonar images and geological interpretation. (a) A small axial volcanic ridge (AVR) which merges along strike with a small fissure. (b) The contact between fresh-looking volcanic constructions and densely faulted terrain.

little deformation. The episode of volcanic construction probably starts with a small volcanic ridge (Figure 11a) resulting from a single or a few eruptions. This primary AVR then grows during successive eruptions up to a final size (500 m for segment 10 and 800 m for segment 17) depending on the volume of magma available (Figures 5 and 10). During this stage of volcanic construction, diking events are frequent, interrupting and sometimes resetting the build-up of tensional stresses perpendicular to the ridge by plate spreading [*Perfit and Chadwick*, 1998]. However, the tectonic cycle of faulting may be only partly short-circuited as small faults and/or fissures are often observed on fresh-looking volcanic constructions which themselves seem to overlay more densely faulted volcanic units (Figure 11b). When magma supply decreases, tectonic processes become predominant: less frequent dike injections in the crust give way to the accumulation of tensional stresses leading to formation of small to large faults [*Perfit and Chadwick*, 1998] as observed on the AVR of segment 17. This AVR is cut on its top by a small graben, its northern side is cut by few large throw faults whereas numerous smaller-scale faults affect the southern side. This example shows that the tectonic deformation is not necessarily focused but may be distributed. When tectonic processes are focused, the AVR is split in half by normal faulting, the two parts are moved apart and a new AVR can latter form in the middle (Figure 10), as observed in segment 16. In case of segment 16 the two parts are not yet moved to the flanks but remain in the axial valley due to the obliquity of the ridge. These previous AVRs are still affected by tectonic processes that occurred in the axial valley resulting in totally dismembered ridges. Normal faulting may occur either on the top of the AVR or on one flank of the AVR resulting in two abyssal hills with different sizes.

5.2. Influence of the Magma Supply on AVR Development

[21] Off-axis bathymetric data, at segments 20 and 21, show that most abyssal hills have a distinctly asymmetric shape, with steep faulted scarps facing toward the axis and gentle dipping volcanic slope facing away (Figure 7). These observations suggest that their formation is due to alternating periods of volcanic construction and tectonic dismemberment. Furthermore, these abyssal hills have almost the same size suggesting that similar volumes of magma were transported to the surface to build these hills. The almost constant distance between successive abyssal hills indicates that the magmato-tectonic cycle is a pseudoperiodic process. The estimation of the period of volcanic construc-

tion obtained from the TOBI data (0.1–0.6 m.y.) to the west of the Melville FZ agrees with the occurrence of abyssal hills every 0.4 m.y in segments 20 and 21. Regular successions of abyssal hills, with similar sizes to the ones on the flanks of segments 20 and 21, are also observed on the flanks of the two segments to the east of the Atlantis II FZ [*Hosford et al.*, 2002, 2003]. The magmato-tectonic cycle inferred from the off-axis pattern of segments 20 and 21 may thus be a common process to all the segments in the oblique SWIR section between the Gallieni and Melville FZs. Both the regularity of the abyssal hills pattern and the almost constant magma supply, indicated by the small amplitude of the crustal thickness variations on the flanks of segment 20 and 21, may be related to the stability of the segmentation which characterizes this ridge section. A highly segmented plate geometry, with large and long discontinuities, exists indeed since 40 m.y. between the Gallieni and Melville FZs [*Sauter et al.*, 2001]. Thick and cold lithosphere at such large discontinuities is believed to depress the top of the melting region and create a gradient at the base of the lithosphere that can focus melt toward the segment centers [*Magde and Sparks*, 1997]. Long-lived large discontinuities may thus contribute to the stability of this focusing mechanism resulting in a regular magma feeding of the segments although the overall magma supply is low in this SWIR section. Nevertheless, this does not preclude episodic formation of buoyant mantle diapirs [*Schouten et al.*, 1985] which may explain the small crustal thickness variations observed every ~3 m.y on the flanks of segment 20 and 21. The availability of melt beneath these segments also controls the repeated injections of magma through dike intrusions which propagate up to the seafloor and feed the axial volcanic ridges. Melt gathers beneath the segments until an excess magma pressure is reached in the melt-rich region and dikes are initiated. The abyssal hill pattern may thus also partly reflect the periodicity of the dike intrusion process together with the variations of the ambient tensional stress perpendicular to the ridge.

[22] The off-axis data of segment 27 in the shallow SWIR section west of the Gallieni FZ show much larger abyssal hills than those observed in the oblique SWIR section between the Gallieni and Melville FZs (Figures 5 and 7). Using the width of these hills, the magmato-tectonic cycle for segment 27 lasts about 1.7–2.7 m.y., 4 to 6 times longer than for segments 20–21. Such large topographic features have also been recognized on the flanks of segment 45 (Figures 1 and 5) which is located in the shallowest SWIR section near the Marion hot spot. We thus propose that higher magma supply, in these shallow ridge sections, may produce larger abyssal hills. A simple model of mantle melting and regional isostatic compensation suggests indeed that differences in mantle temperature and in melt thickness between the oblique section to the east of the Gallieni FZ and the shallower region to the west are of the order of 60°C and 3 km, respectively [*Cannat et al.*, 1999]. C. M. Meyzen et al. (manuscript in preparation, 2003) obtained similar estimations from the Na_8 content of basaltic glasses dredged in these ridge sections. A significantly larger magma supply may increase the frequency of sill intrusion in the crust and develop a shallow magma chamber [*Gudmunsson*, 1990] large enough to initiate multiple injections of dikes. These dikes then feed numerous fissure eruptions which finally result in the building of large volcanic constructions. A more robust magma supply may also cause episodic volcanic burial of topographic lows which could explain the present-day absence of both an axial valley and an AVR at segments 27 and 45. A hotter mantle and higher magma supply also favor along-axis melt distribution in the crust and thus longer abyssal hills like those of segment 27. However, the regular off-axis pattern of segment 27 is only observed for a short period of time (~6 m.y.), since the formation of the shallow central domain of the western off-axis survey area. This off-axis pattern may thus not be representative of the long term evolution of a segment with high magma supply. Moreover, discontinuities to the west of the Gallieni FZ are short-lived and smaller than in the oblique ridge section to the east of the Gallieni FZ resulting in less lithospheric control on the melt migration at depth. They bound low-relief segments with thin crust where the magma supply may be controlled by melt migration from the adjacent high relief seg-

ment 27 [*Sauter et al.*, 2001]. An irregular and intermittent feeding of such magmatically weak segments could explain the presence of only a few short series of small abyssal hills on the flank of these segments.

[23] When magma supply strongly decreases and becomes highly discontinuous, as observed outside the shallow central domain to the west of the Gallieni FZ, regular abyssal hill patterns are no longer observed and give way to randomly distributed bathymetric highs. These highs look like those identified by Cannat et al. (submitted manuscript, 2003) in the deep magma-poor section of the SWIR to the east of the Melville FZ. These authors propose that these highs are large volcanic constructions which were initiated by strong and transient melt focusing and fed by rapid melt extraction through dikes. Deep-reaching normal faults then disrupt these constructions leading to the formation of asymmetric seafloor topography. Segment 11 receives indeed more melt than the low regional average (Cannat et al., submitted manuscript, 2003) and displays a fresh looking axial valley which is partly filled, like the magmatically robust segments in the shallowest SWIR section. On the contrary, the absence of significant melt supply beneath the axis at segment 9 could explain the complete tectonic dismemberment of the axial valley which is observed in the TOBI data. This ultimate stage of the evolution of the axial valley may thus be specific to the deep and magma-poor parts of the SWIR where the magma supply is highly episodic and nonstatic.

6. Conclusions

[24] 1. Side scan sonar images of the SWIR segments allow observation of fresh-looking unfaulted AVRs, partially faulted AVRs and totally dismembered axial ridges. These various degrees of deformation and differences in the length and height of the AVRs suggest different stages in an evolutionary life cycle of AVR development.

[25] 2. Off-axis bathymetric data, in the oblique SWIR section between the Gallieni and Melville FZs, show that the abyssal hills all display an asymmetric shape, with steep faulted scarps facing toward the axis and gentle dipping volcanic slope facing away. We suggest that their formation is due to successive periods of volcanic construction and tectonic dismemberment.

[26] 3. Large abyssal hills in ridge sections with thicker crust suggest that the magma supply controls the size of the abyssal hills. The regular spacing between the abyssal hills in ridge sections of thinner crust suggests that the magmato-tectonic cycle is a pseudoperiodic process which lasts ~0.4 m.y., about 4 to 6 times shorter than in ridge sections of thicker crust (1.7–2.7 m.y.).

[27] 4. We suggest that the regularity of the abyssal hills pattern, observed in the oblique SWIR section, is related to the persistence of a nearly constant magma supply beneath long-lived segments. By contrast, when magma supply strongly decreases and becomes highly discontinuous, regular abyssal hills patterns are no longer observed.

Acknowledgments

[28] We thank Catherine Mével and Kensaku Tamaki for organizing the FUJI cruise. We want to thank Yvon Balut and Commandant Patrick Regnier, officers and crew of the R/V Marion Dufresne for their assistance during the FUJI cruise. We also thank Commandant G. Tredunit, officers and crew of the R/V L'Atalante for their assistance during the Gallieni cruise. We are grateful to Eric Humler for inviting D. Sauter on the SWIFT cruise. We want to thank Nancy Grindlay, William Chadwick and Catherine Mével for their helpful reviews. Figures were created using the public-domain GMT software [*Wessel and Smith*, 1991]. V. Mendel benefited from a EC-TMR Marie Curie fellowship and a "Société de Secours des Amis des Sciences" grant. This is EOST contribution N° 2002.18-UMR7516.

References

Bown, J. W., and R. S. White, Variation with spreading rate of oceanic crustal thickness and geochemistry, *Earth Planet. Sci. Lett.*, *121*, 435–449, 1994.

Briais, A., H. Sloan, L. M. Parson, and B. J. Murton, Accretionary processes in the axial valley of the Mid-Atlantic Ridge 27°N–30°N from TOBI side-scan sonar images, *Mar. Geophys. Res.*, *21*, 87–119, 2000.

Buck, W. R., and A. N. B. Poliakov, Abyssal hills formed by stretching oceanic lithosphere, *Nature*, *392*, 272–275, 1998.

Cande, S. C., and D. V. Kent, Revised calibration of the geomagnetic polarity timescale for the Late Cretaceous and Cenozoic, *J. Geophys. Res.*, *100*, 6093–6096, 1995.

Cannat, M., C. Rommevaux-Jestin, D. Sauter, C. Deplus, and V. Mendel, Formation of the axial relief at the very slow spreading Southwest Indian Ridge (49° to 69°E), *J. Geophys. Res.*, *104*, 22,825–22,843, 1999.

DeMets, C., R. G. Gordon, D. F. Argus, and S. Stein, Current plate motions, *Geophys. J. Int.*, *101*, 425–478, 1990.

Flewellen, C. G., N. W. Millard, and I. P. Rouse, TOBI, a vehicle for deep ocean survey, *J. Electron. Commun. Eng.*, *5*, 85–93, 1993.

Georgen, J. E., J. Lin, and H. J. B. Dick, Evidence from gravity anomalies for interactions of Marion and Bouvet hotspots with the Southwest Indian Ridge: Effects of transform offsets, *Earth Planet. Sci. Lett.*, *187*, 283–300, 2001.

Gràcia, E., L. M. Parson, D. Bideau, and R. Hekinian, Volcano-tectonic variability along segments of the Mid-Atlantic Ridge between Azores platform and Hayes fracture zone: Evidence from submersible and high-resolution sidescan sonar data, in *Modern Ocean Floor Processes and the Geological Record*, edited by R. A. Mills and K. Harrison, *Geol. Soc. Spec. Publ., 148*, 1–15, 1998.

Grindlay, N. R., J. A. Madsen, C. Rommevaux, J. Sclater, and S. Murphy, Southwest Indian Ridge 15°E–35°E: A geophysical investigation of an ultra-slow spreading mid-ocean ridge system, *InterRidge News*, *5*, 7–12, 1996.

Gudmunsson, A., Emplacement of dykes, sills and crustal magma chambers at divergent plate boundaries, *Tectonophysics*, *176*, 257–275, 1990.

Hosford, A., H. Dick, M. Tivey, J. Lin, and T. Matsumoto, A 25 Myr record of crustal accretion at the SWIR between the Atlantis II (57°E) and Novara (58°30′E) fracture zones (abstract), paper presented at InterRidge South West Indian Ridge Workshop, InterRidge, Southampton, U.K., 2002.

Hosford, A., M. Tivey, T. Matsumoto, H. Dick, H. Schouten, and H. Kinoshita, Crustal magnetization and accretion at the Southwest Indian Ridge near the Atlantis II fracture zone, 0–25 Ma, *J. Geophys. Res.*, *108*(B3), 2169, doi:10.1029/2001JB000604, 2003.

Humler, E., et al., Campagne SWIFT sur la dorsale Sud Ouest Indienne entre 30°E et 50°E (N. O. Marion Dufresne, du 14 février au 21 mars 2001): Caractérisation géophysique et géochimique, *Lett. Dorsales*, *8*(1–2), 10–14, 2001.

Kappel, E. S., and W. B. F. Ryan, Volcanic episodity and a non-steady state rift valley along northeast Pacific spreading centers: Evidence from Seamarc I, *J. Geophys. Res.*, *91*, 13,925–13,940, 1986.

Louden, K. E., J. C. Osler, S. P. Srivastava, and C. E. Keen, Formation of oceanic crust at slow spreading rates: New constraints from an extinct spreading center in the Labrador Sea, *Geology*, *24*, 12,197–12,225, 1996.

MacDonald, K. C., P. J. Fox, R. T. Alexander, R. A. Pockalny, and P. Gente, Volcanic growth faults and the origin of Pacific abyssal hills, *Nature*, *380*, 125–129, 1996.

Magde, L. S., and D. W. Sparks, Three-dimensional mantle upwelling, melt generation, and melt migration beneath segment slow spreading ridges, *J. Geophys. Res.*, *102*, 20,571–20,583, 1997.

Malinverno, A., and R. A. Pockalny, Abyssal hill topography as an indicator of episodicity in crustal accretion and deformation, *Earth Planet. Sci. Lett.*, *99*, 154–169, 1990.

Mendel, V., D. Sauter, L. Parson, and J.-R. Vanney, Segmentation and morphotectonic variations along a super slow-spreading center: The Southwest Indian Ridge (57°E–70°E), *Mar. Geophys. Res.*, *19*, 505–533, 1997.

Mével, C., and EDUL Shipboard Scientific Party, EDUL cruise report, R/V Marion Dufresne 107, 184 pp., Lab. de Pétrol., Univ. Paris VI, 1997.

Meyzen, C. M., M. J. Toplis, E. Humler, J. N. Ludden, and C. Mével, A major discontinuity in mantle composition beneath the Southwest Indian Ridge, *Nature*, *421*, 731–733, 2003 .

Muller, M. R., T. A. Minshull, and R. S. White, Segmentation and melt supply at the Southwest Indian Ridge, *Geology*, *27*, 867–870, 1999.

Parson, L. M., et al., En echelon axial volcanic ridges at the Reykjanes Ridge: A life cycle of volcanism and tectonics, *Earth Planet. Sci. Lett.*, *117*, 73–87, 1993.

Patriat, P., et al., The GALLIENI cruise: A geophysical survey of the South-West Indian Ridge near the Gallieni FZ (37°S, 52°E), *InterRidge News*, *5*, 19–22, 1996.

Patriat, P., D. Sauter, M. Munschy, and L. Parson, A survey of the Southwest Indian Ridge axis between Atlantis II FZ and the Indian Ocean Triple Junction: Regional setting and large scale segmentation, *Mar. Geophys. Res.*, *19*, 457–480, 1997.

Perfit, M. R., and W. W. Chadwick, Magmatism at mid-ocean ridges: Constraints from volcanological and geochemical investigations, in *Faulting and Magmatism at Mid-Ocean Ridges*, *Geophys. Monogr. Ser.*, vol. 106, edited by W. R. Buck et al., pp. 59–115, AGU, Washington, D. C., 1998.

Pezard, P. A., R. N. Anderson, W. B. F. Ryan, K. Becker, J. C. Alt, and P. Gente, Accretion, structure and hydrology of intermediate spreading-rate oceanic-crust from drillhole experiments and seafloor observations, *Mar. Geophys. Res.*, *14*, 93–123, 1992.

Pockalny, R. A., R. S. Detrick, and P. J. Fox, Morphology and tectonics of the Kane transform from Sea beam bathymetric data, *J. Geophys. Res.*, *93*, 3179–3193, 1988.

Poliakov, A. N. B., and W. R. Buck, Mechanics of stretching elastic-plastic-viscous layers: Applications to slow-spreading mid-ocean ridges, in *Faulting and Magmatism at Mid- Ocean Ridges*, *Geophys. Monogr. Ser.*, vol. 106, edited by W. R. Buck et al., pp. 305–323, AGU, Washington, D. C., 1998.

Robinson, C. J., R. S. White, M. J. Bickle, and T. A. Minshull, Restricted melting under the very slow-spreading Southwest Indian Ridge, in *Tectonic, Magmatic, Hydrothermal and Biological Segmentation of Mid-Ocean Ridges*, edited by C. J. MacLeod, P. A. Tyler, and C. L. Walker, *Geol. Soc. Spec. Publ., 118*, 131–141, 1996.

Rommevaux, C., C. Deplus, and P. Patriat, Three-dimensional gravity study of the Mid- Atlantic Ridge: Evolution of the segmentation between 28° and 29°N during the last 10 m.y., *J. Geophys. Res.*, *99*, 3015–3029, 1994.

Sauter, D., P. Patriat, C. Rommevaux-Jestin, M. Cannat, and A. Briais, The Southwest Indian Ridge between 49°15′E and

57°E: Focused accretion and magma redistribution, *Earth Planet. Sci. Lett.*, *192*, 303–317, 2001.

Sauter, D., L. Parson, V. Mendel, C. Rommevaux-Jestin, O. Gomez, A. Briais, C. Mével, and K. Tamaki, TOBI sidescan sonar imagery of the very slow- spreading Southwest Indian Ridge: Evidence for along-axis magma distribution, *Earth Planet. Sci. Lett.*, *199*, 81–95, 2002a.

Sauter, D., et al., Scale, nature and origin of the segmentation of the Southwest Indian Ridge from the Prince Edward transform fault to the Rodrigues triple junction (abstract), paper presented at InterRidge South West Indian Ridge Workshop, InterRidge, Southampton, U.K., 2002b.

Schouten, H., K. D. Klitgord, and J. A. Whitehead, Segmentation of the mid-ocean ridges, *Nature*, *317*, 225–229, 1985.

Smith, D. K., et al., Mid-Atlantic Ridge volcanism from deep-towed side-scan sonar images, 25°–29°N, *J. Volcanol. Geotherm. Res.*, *67*, 233–262, 1995.

Smith, W. H. F., and D. T. Sandwell, Marine gravity field from declassified Geosat and ERS-1 altimetry, *Eos Trans. AGU*, *76*(46), Fall Meet. Suppl., 156, 1995.

Sotin, C., and E. M. Parmentier, Dynamical consequences of compositional and thermal density stratification beneath spreading centers, *Geophys. Res. Lett.*, *16*, 835–838, 1989.

Tamaki, K., C. Mével, and the FUJI Scientific Party, Spreading tectonics of the eastern part of the Southwestern Indian Ridge: A synthesis of FUJI expedition (abstract), *Eos Trans. AGU*, *79*(45), Fall Meet. Suppl., F892, 1998.

Wessel, P., and W. H. F. Smith, Free software helps map and display data, *Eos Trans. AGU*, *72*, 441, 1991.